Infrared Spectra of Thallium Hydrides in Solid Neon, Hydrogen, and Argon

Xuefeng Wang and Lester Andrews*

Department of Chemistry, University of Virginia, McCormick Road, P.O. Box 400319, Charlottesville, Virginia 22904-4319

Received: January 8, 2004; In Final Form: February 10, 2004

Laser-ablated Tl atoms react with dihydrogen in excess neon, pure hydrogen, and excess argon to form primarily the TlH diatomic molecule. Ultraviolet irradiation increases weak bands that are identified as TlH_2 and TlH_3 on the basis of D_2 and HD substitution and density functional theory (DFT) isotopic frequency calculations. Sample annealing fosters the dimerization of TlH to give Tl_2H_2 with a rhombic ring structure and the $TlTlH_2$ isomer. The markedly lower yield of TlH_3 in these experiments compared to AlH_3 in earlier investigations is due to the expected decrease in stability for the Tl(III) oxidation state. The $Tl^+(H_2)_n$ cation complex is also observed, and trends within the group 13 metals are summarized. Excitation at 193 nm gives the $^2S_{1/2} \rightarrow {}^2P_{1/2,3/2}$ doublet for unreacted Tl atoms, which is blue-shifted 660 cm^{-1} from the gas-phase value in solid D_2 but only 210 cm^{-1} in solid H_2, owing to the smaller, more repulsive D_2 matrix cage.

Introduction

Small group 13 metal hydrides have been investigated extensively (M = Al, Ga, or In), including by gas-phase spectroscopy for the monohydride diatomics[1−9] and matrix infrared studies for the mono-, di-, and trihydrides, which reveal increasing frequencies in the $MH_{1,2,3}$ series for each metal.[10−18] Electron spin resonance has been employed to investigate the AlH_2 radical in solid neon.[19] The M_2H_2 and M_2H_6 species have been characterized by increasing stability of the former and decreasing stability of the latter with the heavier metals. Thallium hydride, TlH, has only been investigated in the gas phase,[1,20] and by theoretical calculations,[21−24] and there is no experimental evidence to date for TlH_2 and TlH_3, although the latter have also been subjected to theoretical calculations as heavy metal compounds, owing to interest in relativistic effects.[25,26] The trend of decreasing stability for the heavier metal trihydride is manifest in the lower yield of InH_3 relative to AlH_3,[18] and this points to difficulty for the preparation of TlH_3.

Experimental and Theoretical Methods

The laser-ablation matrix-isolation infrared spectroscopy experiment has been described previously.[27,28] Briefly, the Nd:YAG laser fundamental (1064 nm, 10 Hz repetition rate, 10 ns pulse width) was focused on rotating a high purity thallium (Spex Industries, 99.999%) target using 5−20 mJ/pulse, and thallium atoms were co-deposited with pure H_2 or D_2 (Matheson), pure HD (Cambridge Isotope Laboratories), and neon or argon diluted samples onto a CsI window cooled to 3.5 K by a Sumitomo Heavy Industries RDK-205D cryocooler. Infrared spectra were recorded in a Nicolet 750 Fourier transform instrument at 0.5 cm^{-1} resolution using a liquid-nitrogen cooled MCTB detector after deposition, annealing, and filtered mercury arc or 193 nm laser (Lambda Physik, Optex) irradiation. Emission spectra were recorded using an Ocean Optics optical fiber spectrometer.

* To whom correspondence should be addressed. E-mail: lsa@virginia.edu.

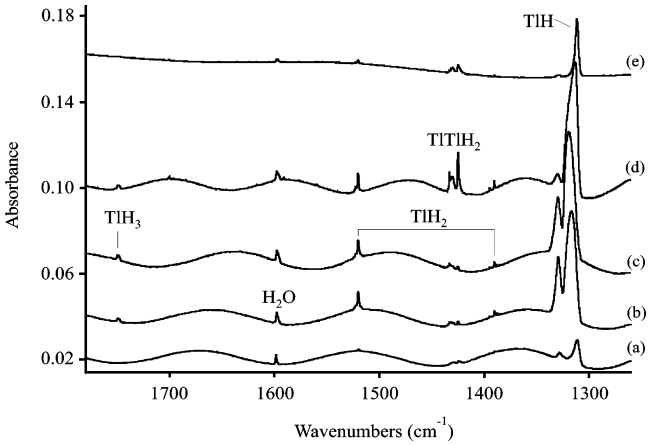

Figure 1. Infrared spectra in the 1780−1260 cm^{-1} region for normal hydrogen co-deposited at 3.5 K with laser-ablated thallium. Spectra of H_2 + Tl: (a) before irradiation, (b) after 15 min of $\lambda > 240$ nm irradiation, (c) after 15 min more of $\lambda > 240$ nm irradiation, (d) after annealing to 6.0 K, and (e) after annealing to 6.5 K.

Density functional theory (DFT) frequency calculations were helpful in assigning lead and bismuth hydride spectra,[29,30] so similar B3LYP/6-311++G**/Stuttgart scalar relativistic pseudopotential for Tl together with the corresponding basis set (SDD) calculations were performed for thallium hydrides using the Gaussian 98 program system.[31−33] Comparable results were obtained using the BPW91 functional.[34] Although these calculations are only approximate, they provide a useful guide for assigning vibrational spectra.

Results

Reaction products from laser-ablated Tl and dihydrogen trapped in excess hydrogen, neon, and argon and supporting DFT calculations will be presented.

Hydrogen. Laser-ablated Tl co-deposited with hydrogen (deuterium) produces weak bands at 1311 (940) cm^{-1} that increase upon ultraviolet irradiation to strong bands at 1311.3 (939.9) cm^{-1}, as shown in Figure 1 (Figure 2). This treatment

10.1021/jp0498973 CCC: $27.50
Published on Web 03/19/2004

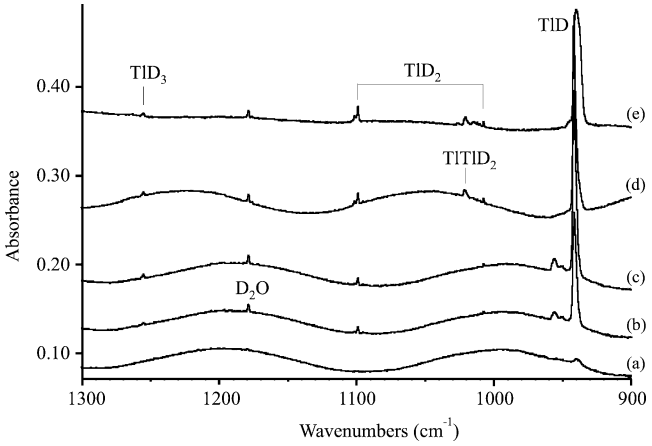

Figure 2. Infrared spectra in the 1300−900 cm^{-1} region for normal deuterium co-deposited at 3.5 K with laser-ablated thallium. Spectra of D_2 + Tl: (a) before irradiation, (b) after 15 min of $\lambda > 240$ nm irradiation, (c) after 15 min more of $\lambda > 240$ nm irradiation, (d) after annealing to 8.0 K, and (e) after annealing to 9.0 K.

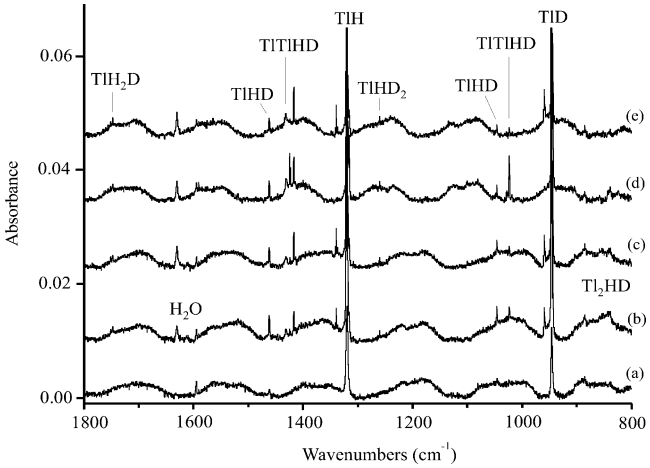

Figure 3. Infrared spectra in the 1800−800 cm^{-1} region for pure HD co-deposited at 3.5 K with laser-ablated thallium. Spectra of HD + Tl: (a) before irradiation, (b) after 30 min of $\lambda > 240$ nm irradiation, (c) after annealing to 7.3 K, (d) after 15 min of $\lambda > 240$ nm irradiation, and (e) after annealing to 8.0 K.

also yields new absorptions at 1519.9 (1098.8) and 1390.2 (1007.6) cm^{-1} and weak bands at 1748.4 (1254.4) cm^{-1}. Annealing increases the strong bands and new features at 1424.3 (1020.5) cm^{-1}. Weak bands also appear upon annealing at 908.8 (653.1) cm^{-1} that are produced in greater yield using neon host matrixes. Table 1 lists the observed frequencies.

The HD experiment provides important diagnostic information on the thallium hydrides in Figure 3. The strong initial bands are observed slightly shifted in the pure HD host at 1320.1 and 945.9 cm^{-1}. The sharp 1519.9 (1098.8) and 1390.2 (1007.6) cm^{-1} bands are replaced by a new set at 1461.8 and 1046.2 cm^{-1}. The weaker 1748.4 (1254.4) cm^{-1} absorptions shift to 1747.3 and 1258.1 cm^{-1}. Finally, a weak 839.0 cm^{-1} band is observed instead of the 908.8 (653.1) cm^{-1} pair.

The higher frequency region for hydrogen (deuterium) reveals sharp new 4113.6 (2962.8) cm^{-1} absorptions and other metal independent absorptions observed previously at 4143.4 (2982.4) and 3972 (2870) cm^{-1}.[16−18] The spectra in Figure 4 show that $\lambda > 240$ nm irradiation effectively destroys all product bands in this region. However, in the more robust deuterium lattice, the 2870 cm^{-1} absorption for $(D^-)(D_2)_n$ is regenerated in part by 193 nm irradiation: this destruction−regeneration cycle is repeated. Likewise, the higher frequency region with HD shows analogous sharp bands at 3621.7 and 3596.3 cm^{-1} and a broader feature at 3478 cm^{-1}. The sharp 3621.7 cm^{-1} and broad 3478 cm^{-1} bands are common to other metal experiments with HD.

Neon. Weak bands are observed at 1327 (950) cm^{-1} for H_2 (D_2) in excess neon co-deposited with Tl atoms. Spectra in Figure 5 compare deposited samples after deposition and 193 nm irradiation (5 min at 4 mJ/pulse). Stronger bands at 919.8 (667.3) cm^{-1} acquire a 851.1 cm^{-1} HD counterpart. Irradiation also produces weaker 1525.9 (1103.5) cm^{-1} bands with a 1468 cm^{-1} HD counterpart.

TABLE 1: Infrared Absorptions (cm^{-1}) Observed from Reaction of Thallium and Dihydrogen in Neon, Hydrogen, and Argon

neon			hydrogen			argon			
H_2	HD	D_2	H_2	HD	D_2	H_2	HD	D_2	identity
			4113.6	3596.3	2962.8				$Tl^+(H_2)_n$
			1748.4	1747.3					TlH_3
				1259.9	1254.4				TlD_3
			1700.2						anneal pdt
					1224.3				anneal pdt
			1522.4						TlH_2 (site)
1525.9			1519.9			1503.3			TlH_2
	1468			1461.8, 1046.2					TlHD
		1112.3			1101.4				TlD_2 (site)
		1103.5			1098.8			1082.0	TlD_2
			1394.7						TlH_2 (site)
			1390.2						TlH_2
					1010.3				TlD_2 (site)
					1007.6				TlD_2
			1430.3	1430.8					$TlTlH_2$ (site)
1431.7			1424.3	1424.8			1427.6		$TlTlH_2$
				1424.2, 1423.0					TlTlHD
				1023.9, 1022.6					TlTlHD
				1023.5	1021.6				$TlTlD_2$ (site)
				1027.7	1020.5				$TlTlD_2$
			1328.0	1339.6					TlH (site)
1327	1327		1311.3	1320.1		1309.4	1309.4		TlH
				959.4	953.4		938.0		TlD (site)
	950	950		945.9	939.9			938.0	TlD
919.8			908.8			888.2	888.0		Tl_2H_2
	851.1			839.0			825.3		Tl_2HD
		667.3			653.1		642.8	642.6	Tl_2D_2

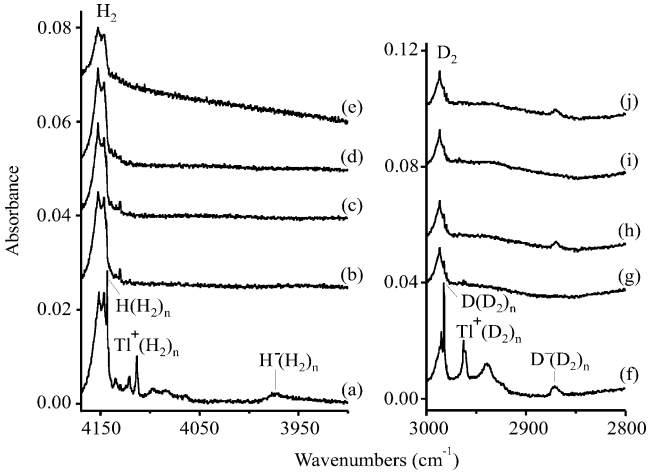

Figure 4. Infrared spectra in the H−H and D−D stretching regions for hydrogen and deuterium co-deposited at 3.5 K with thallium. Spectra of H_2 + Tl: (a) before irradiation, (b) after 15 min of $\lambda > 240$ nm irradiation, (c) after 15 min more of $\lambda > 240$ nm irradiation, (d) after annealing to 6.0 K, and (e) after annealing to 6.5 K. Spectra of D_2 + Tl: (f) before irradiation, (g) after 15 min of $\lambda > 240$ nm irradiation, (h) after 3 min of 193 nm irradiation (5 mJ/pulse at 10 Hz), (i) after $\lambda > 240$ nm irradiation, and (j) after 4 min of 193 nm irradiation.

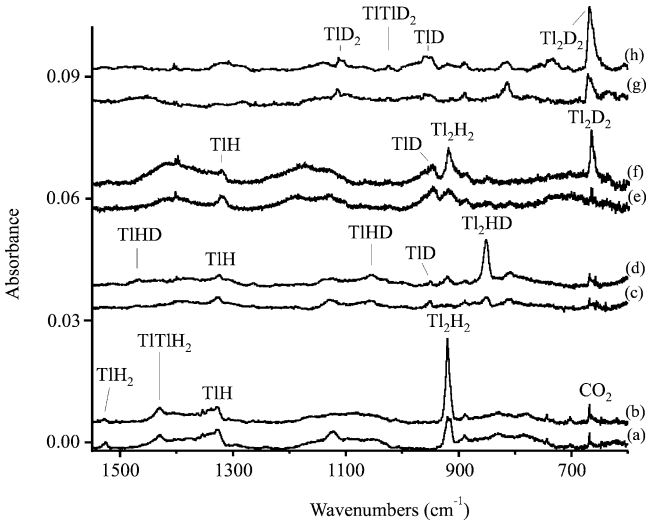

Figure 5. Infrared spectra in the 600−1550 cm^{-1} region for hydrogen co-deposited at 3.5 K with thallium in neon. Spectra of 4% H_2 in neon + Tl: (a) before irradiation and (b) after 5 min of 193 nm (5 mJ/pulse at 10 Hz) irradiation. Spectra of 4% HD in neon + Tl: (c) before irradiation and (d) after 193 nm irradiation. Spectra of 2% H_2 + 2% D_2 in neon + Tl: (e) before irradiation and (f) after 193 nm irradiation. Spectra of 4% D_2 in neon + Tl: (g) before irradiation and (h) after 193 nm irradiation.

Argon. The weak argon matrix H_2 (D_2) reaction products at 1309.4 (938.0) cm^{-1} increase markedly upon annealing to allow diffusion and reaction of trapped atomic species, as shown in Figure 6a,b and i,j. Additional bands appear at 888.2 (642.6) cm^{-1} upon annealing. Using the HD reagent, the latter two bands plus a new 825.3 cm^{-1} absorption are produced: Increased laser energy favors the yield of TlH and TlD, as illustrated in Figure 6c−f. The Ar_nH^+ and Ar_nD^+ species were also trapped in solid argon.[35,36]

Emission Spectra. Emission spectra were recorded from the 1064 nm laser-generated plume above the target surface during ablation−deposition. The strong Tl atomic spin−orbit doublets[37] were observed at 377.7 and 535.2 nm and at 276.9 and 353.0 nm, as shown in Figure 7. In addition, weaker Tl^+ lines were found at 329.1, 507.7, 515.4, and 595.0 nm.[38] During 193 nm irradiation of the H_2 and D_2 samples, strong Tl atomic doublets were observed at 374.7 and 526.2 nm and 368.5 and 513.8 nm, respectively. Similar 193 nm irradiation of neon and argon matrix samples containing Tl and H_2 produced broader features and sharper bands for atomic Tl at 548 nm in the former and 393 and 549 nm in the latter.

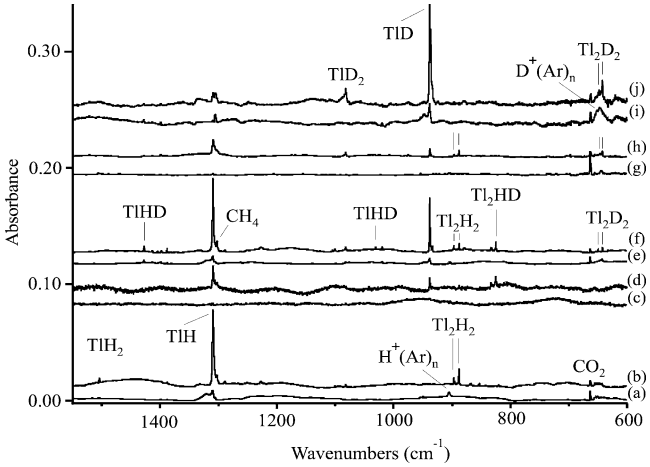

Figure 6. Infrared spectra in the 600−1550 cm^{-1} region for hydrogen co-deposited at 3.5 K with thallium in argon. Spectra of 4% H_2 in argon + Tl: (a) before annealing and (b) after annealing to 30 K. Spectra of 3% HD in argon + Tl (10 mJ/pulse): (c) before annealing and (d) after annealing to 30 K. Spectra of 6% HD in argon + Tl (30 mJ/pulse): (e) before annealing and (f) after annealing to 30 K. Spectra of 1.5% H_2 + 1.5% D_2 in argon + Tl: (g) before annealing and (h) after annealing to 30 K. Spectra of 4% D_2 in argon + Tl: (i) before annealing and (j) after annealing to 30 K.

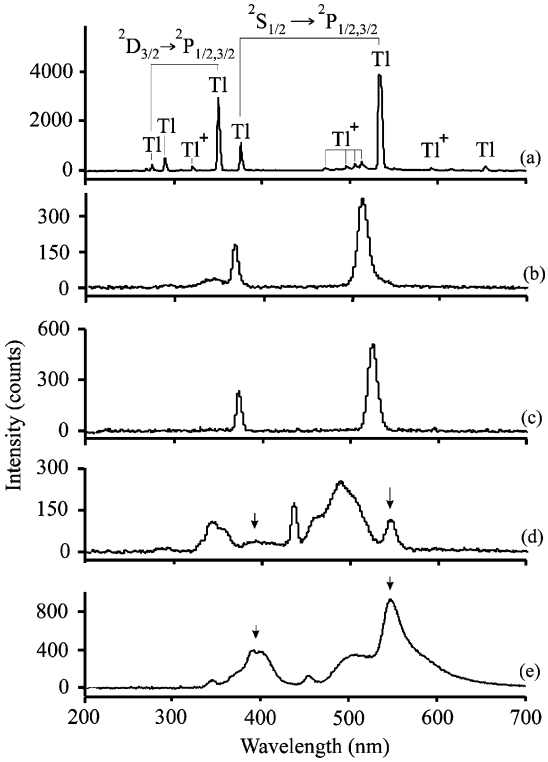

Figure 7. Emission spectra from hydrogen−thallium experiments: (a) emission from the 1064 nm laser-ablation plume, (b) emission from solid D_2 + Tl using 193 nm excitation at 1 mJ/pulse, (c) emission from solid H_2 + Tl using 193 nm excitation at 1 mJ/pulse, (d) emission from neon + Tl using 193 nm excitation, and (e) emission from argon + Tl using 193 nm excitation.

Discussion

New thallium hydride absorptions will be assigned on the basis of isotopic substitution, matrix shifts, and quantum chemical calculations.

TlH. Experiments with laser-ablated Tl and hydrogen (deuterium) gave weak bands at 1311.3 (939.9) cm^{-1}, which increased markedly upon UV irradiation (Figures 1 and 2) and are slightly lower than the gas-phase TlH (TlD) fundamentals[1,20] of 1345.3 (963.7) cm^{-1} and are due to the diatomic hydride molecules in solid H_2 (D_2). These TlH (TlD) bands are bracketed by the argon matrix (1309.4 (938.0) cm^{-1}) and neon matrix (1327 (950) cm^{-1}) values. Two sharp bands were observed with pure HD, but both were blue-shifted 0.6% from the H_2 (D_2) matrix values. Our simple B3LYP calculation predicts 1306 (926) cm^{-1} for these heavy metal hydride frequencies, which is excellent, considering the approximations involved. The BPW91 functional is slightly lower and not in as good agreement.

TlH_2. Weak sharp absorptions are produced at 1519.9 (1098.8) and 1390.2 (1007.6) cm^{-1} upon 193 nm irradiation of solid hydrogen (deuterium) samples with H/D ratios of 1.383 and 1.380. The solid HD sample revealed sharp 1461.8 and 1046.2 cm^{-1} bands, which are 7 cm^{-1} above and below the medians, respectively, for the two hydrogen and deuterium modes. This substantiates assignment of the two bands to antisymmetric and symmetric stretching modes of TlH_2 (TlD_2), where interaction of the Tl−H and Tl−D stretching modes in TlHD forces the two modes apart from the median TlH_2 (TlD_2) values. The stronger antisymmetric mode is observed at 1525.9 cm^{-1} in solid neon and at 1503.3 cm^{-1} in solid argon, which bracket the solid H_2 value.

Our B3LYP calculations predict the two TlH_2 modes at 1530 and 1415 cm^{-1}, which are 0.6 and 1.8% higher than the hydrogen matrix values. On the other hand, our BPW91 computations find values of 1483 and 1354 cm^{-1}, which are 2.4 and 2.6% lower than the observed values. These are the comparisons expected for DFT frequencies.

TlH_3. Weak, sharp bands appear at 1748.4 (1254.4) cm^{-1} upon irradiation of solid H_2 (D_2) samples. With solid HD, these bands shift to 1747.3 and 1258.1 cm^{-1}, which are the effects expected for TlH_2D and $TlHD_2$. Solid molecular hydrogens are required for the product, as no counterparts were observed in solid neon or argon.

B3LYP calculations found a trigonal planar TlH_3 species with a 1719 cm^{-1} antisymmetric mode and a 1.730 Å bond length. Furthermore, our B3LYP calculations also find TlH_2D to be 2.1 cm^{-1} lower than TlH_3 and $TlHD_2$ and 3.3 cm^{-1} higher than TlD_3, which is in excellent agreement with the observed −1.1 and +5.4 cm^{-1} observed isotopic shifts for these mixed isotopic trihydrides. Relativistic MP2 calculations earlier predicted a 1.728 Å distance and a 1741 cm^{-1} frequency,[26] and these higher level calculations are closer to our experimental observation for TlH_3. On the basis of the neon matrix shift for the antisymmetric mode for TlH_2, we expect the gas-phase TlH_3 fundamental to be at 1760 ± 10 cm^{-1}.

Our TlH_3 band absorbance is much less than what we observed for InH_3, which in turn is much less than what we observed for GaH_3 and AlH_3, and is the expected trend.[26] Evaporation of the H_2 (D_2) matrix gave no evidence of broad absorption bands in the 1500−700 cm^{-1} region that might be due to solid thallium hydride. The low yield of TlH_3 and our failure to observe $(TlH_3)_n$ at low temperature probably is due to the inherent instability of Tl(III) hydride, which casts doubt on the claimed synthesis of $(TlH_3)_n$.[39,40]

Tl_2H_2 and $TlTlH_2$. The large yield of TlH in these experiments invites the consideration of dimers. On the basis of observations for Ga_2H_2 and In_2H_2 and calculations from several groups,[41−45] the rhombic dimer is expected to be the minimum energy structure and several higher energy isomers, including $TlTlH_2$, must be considered.

The evidence for Tl_2H_2 is summarized in Figure 5 for neon experiments where the yield is high. The weak band at 919.8 cm^{-1} with H_2 increases markedly upon 193 nm irradiation and shifts to 677.3 cm^{-1} with D_2 (H/D ratio: 1.378). Experiments with a $H_2 + D_2$ mixture give primarily TlH, TlD, Tl_2H_2, and Tl_2D_2 without evidence of the Tl_2HD species. However, an investigation with HD gives a strong intermediate band at 851.1 cm^{-1} and very weak Tl_2H_2 (Tl_2D_2) bands at 918.8 (653.1) cm^{-1}.

In solid argon, the yield of TlH is high after annealing and a sharp doublet is observed for Tl_2H_2 at 897.0 and 888.2 cm^{-1}, which shifts to 648.9 and 642.6 cm^{-1} with D_2 (H/D ratios: 1.382 and 1.382). Using higher laser energy with HD (Figure 6e,f) gives a large yield of TlH and TlD and a statistical yield of Tl_2H_2, Tl_2HD, and Tl_2D_2. However, using lower laser energy with HD (Figure 6d,e) gives a small yield of TlH and TlD and primarily Tl_2HD at 833.0 and 825.3 cm^{-1}.

In solid molecular hydrogen, the weak 908.8 (653.1) cm^{-1} H_2 (D_2) bands are between solid neon and argon values, and pure HD gives an intermediate 839.0 cm^{-1} band. Such is also the case for In_2H_2.[18,41]

Our B3LYP calculations find a very intense b_{1u} mode for rhombic Tl_2H_2 at 915 cm^{-1}, which is in excellent agreement with the 918.8 cm^{-1} neon matrix observation. Stronger interactions with the H_2 and Ar matrixes shift this absorption to lower wavenumbers. The analogous In_2H_2 species absorbs higher at 982.6 cm^{-1} in solid neon. Our B3LYP calculations predict Tl_2D_2 at 648.8 cm^{-1} in the harmonic approximation (H/D ratio: 1.410), and the lower 1.378 neon matrix isotopic frequency ratio is due to anharmonicity in the vibration. Upon symmetry lowering to Tl_2HD, the normal mode changes and our B3LYP calculation predicts the strongest Tl_2HD mode at 832.0 cm^{-1}, 83/266 of the way from the Tl_2H_2 to Tl_2D_2 frequencies. Our observed Tl_2HD band is 70/256 of the way from the neon matrix Tl_2H_2 to Tl_2D_2 values.

Annealing increases sharp new bands at 1430.8 and 1424.3 cm^{-1} in H_2 with a weaker 1020.5 cm^{-1} D_2 counterpart: the H/D ratio 1.396 is slightly higher than the values for the nearby TlH_2 absorptions. The growth upon annealing invites consideration of another Tl_2H_2 isomer. Calculations for the Ga and In analogues[17,18,41] show that the C_{2v} MMH_2 isomer is next in energy, but our DFT calculations find the C_s isomer next with the C_{2v} and C_{2h} isomer energies within 6 kcal/mol. However, the observed frequencies match best for the C_{2v} $TlTlH_2$ isomer (Table 2). Annealing increases split bands at 1424.2 and 1423.0 cm^{-1} and at 1023.5 and 1022.6 cm^{-1} in pure HD that show the small sretch−stretch interaction calculated for the $TlTlH_2$ isomer. Our B3LYP calculation predicts close b_2 and a_1 modes, and the 1430.8 and 1424.3 cm^{-1} bands are assigned accordingly.

$Tl^+(H_2)_n$. The sharp bands at 4113.6 (2962.8) cm^{-1} (Figure 4) decrease upon full arc irradiation, never to return. An intermediate 3596.3 cm^{-1} counterpart is observed with pure HD. The former absorptions follow a series of like bands with Al (4108.7 and 2959.4 cm^{-1}), Ga (4108.9 and 2960.4 cm^{-1}), and In (4113.1 and 2961.9 cm^{-1}) for the metal cation trapped in the solid molecular hydrogen lattice and the resulting perturbation on the solvating H_2 (D_2) ligand vibration. The small metal dependence on this species arises from the weak interaction. Our B3LYP calculation shows that the side-bound $Tl^+(H_2)$

TABLE 2: Calculated Structures and Vibrational Frequencies (cm^{-1}) for Thallium Hydrides

species	state	structure: bond length, Å, or angle, deg	rel energy, kcal/mol	frequencies, cm^{-1} (sym, intensities, km/mol)
				B3LYP/6-311++G(d,p)/LanL2DZ
TlH ($C_{\infty v}$)	$^1\Sigma$	TlH: 2.024		TlH: 1236.4 (1206). TlD: 876.7 (606)
TlH_2 (C_{2v})	$^2A_1$	TlH: 1.929		TlH_2: 1355.6 (b_2, 642), 1214.6 (a_1, 231), 506.4 (a_1, 95)
		HTlH: 120.2		TlD_2: 962.4 (324), 860.2 (117), 359.5 (48)
TlH_3 (D_{3h})	$^1A_1'$	TlH: 1.830		TlH_3: 1657.7 (a_1', 0), 1645.6 (e′, 498 × 2), 564.8 (a_2'', 200), 531.8 (e′, 229 × 2)
				B3LYP/6-311++G(d,p)/SDD
TlH ($C_{\infty v}$)	$^1\Sigma$	TlH: 1.905		TlH: 1306.0 (1159). TlD: 926.1 (583)
TlH_2 (C_{2v})	$^2A_1$	TlH: 1.787	0.0	TlH_2: 1530.8 (b_2, 660), 1415.3 (a_1, 178), 616.3 (a_1, 133)
		HTlH: 121.9		TlD_2: 1086.9 (333), 1002.1 (90), 437.7 (67)
TlH_2^- (C_{2v})	$^1A_1$	TlH: 1.988	−32.3	TlH_2^-: 1029.6 (a_1, 1880), 1019.4 (b_2, 2016), 622.5 (a_1, 78)
		HTlH: 91.8		TlD_2^-: 730.2 (942), 722.9 (1009), 441.3 (37)
$Tl^+(H_2)$ (C_{2v})	$^1A_1$	TlH: 3.126	103	$Tl^+(H_2)$: 4369.5 (a_1, 52), 195.4 (b_2, 17), 193.8 (a_1, 13)
		HH: 0.747		$Tl^+(D_2)$: 3090.9 (26), 138.3 (8), 137.7 (7)
TlH_2^+ ($D_{\infty h}$)	$^1\Sigma_g^+$	TlH: 1.660	150	TlH_2^+: 2054.2 (σ_u, 15), 1961.7 (σ_g, 0), 713.7 (π_u, 30 × 2)
		HTlH: 180.0		TlD_2^+: 1460.1 (8), 1387.7 (0), 507.3 (16 × 2)
TlH_3 (D_{3h})	$^1A_1'$	TlH: 1.730		TlH_3: 1753.5 (a′, 0), 1718.8 (e′, 445 × 2), 666.6 (a_2'', 181), 614.1 (e′, 210 × 2)
		HTlH: 120.0		TlD_3: 1240.4 (0), 1219.5 (227 × 2), 475.0 (92), 436.2 (106 × 2)
				TlH_2D: 1742.2 (142), 1716.7 (463), 1229.6 (136), 612.6 (214), 609.5 (151), 503.0 (139)
				$TlHD_2$: 1728.7 (306), 1233.0 (84), 1222.8 (206), 559.8 (178), 546.4 (122), 436.5 (105)
TlH_4^- (T_d)	$^1A_1$	TlH: 1.807		TlH_4^-: 1536.0 (a_1, 0), 1415.5 (t_2, 956 × 3), 642.1 (e, 0 × 2), 608.0 (t_2, 583 × 3)
				TlD_4^-: 1086.6 (0), 1003.4 (483 × 3), 454.2 (0 × 2), 433.3 (288 × 3)
Tl_2H_2 (D_{2h})	^1A_g	TlH: 2.157	0.0	Tl_2H_2: 982.0 (a_g, 0), 914.9 (b_{1u}, 2435), 707.9 (b_{2u}, 491), 664.1 (b_{3g}, 0), 303.3 (b_{3u}, 11), 95.0 (a_g, 0)
		HTlH: 109.9		Tl_2HD: 891.7 (114), 832.0 (1714), 552.1 (255), 517.5 (116), 262.5 (8), 95 (0)
				Tl_2D_2: 694.8 (0), 648.8 (1224), 502.0 (247), 470.3 (0), 215.1 (60), 95.0 (0)
Tl_2H_2 (C_s)	$^1A'$	TlH: 1.845	12.4	Tl_2H_2: 1381.6 (a′, 1293), 1003.7 (a′, 506), 592.6 (a′, 674), 318.6 (a′, 5), 196.1 (a″, 5), 50.7 (a′, 2)
		TlH′: 2.340		
		TlTl′: 3.285		
		Tl′H′: 2.041		
		HTlH′: 99.2		
Tl_2H_2 (C_{2h})	^1A_g	TlH: 1.867	17.3	Tl_2H_2: 1358.0 (b_u, 2193), 1350.7 (a_g, 0), 333.6 (a_g, 0), 130.9 (a_u, 48), 40.7 (a_g, 0), 35.4 (b_u, 14)
		TlTl: 3.352		
		TlTlH:		
Tl_2H_2 (C_{2v})	$^1A_1$	TlH: 1.793	18.2	Tl_2H_2: 1508.4 (b_2, 710), 1505.8 (a_1, 1069), 642.7 (a_1, 498), 315.1 (b_1, 81), 160.8 (b_2, 35), 87.6 (a_1, 4)
		TlTl′: 3.129		
		HTlH: 107.9		
Tl_2H_6 (D_{2h})	^1A_g	TlH: 2.012		Tl_2H_6: 1833.3 (b_{2u}, 653), 1828.6 (a_g,0), 1824.9 (b_{3u}, 164), 1824.0 (b_{1g}, 0),
		TlH′: 1.700		1186.5 (a_g, 0), 1078.2 (b_{3u}, 1333), 1001.3 (b_{2g}, 0), 914.3 (b_{1u}, 460),
		TlHTl: 100.7		680.1 (b_{2u}, 196), 648.9 (b_{3g}, 0), 611.1 (a_g, 0), 606.5 (b_{1u}, 109), 503.8 (b_{3u}, 972),
		H′TlH′: 137.1		401.5 (b_{1g}, 0), 368.8 (a_u, 0), 196.3 (b_{2u}, 0), 134.3 (b_{2g}, 0), 107.8 (a_g, 0)
				BPW91/6-311++G(d,p)/SDD
TlH ($C_{\infty v}$)	$^1\Sigma$	TlH: 1.923		TlH: 1278.3 (1039). TlD: 906.4 (522)
TlH_2 (C_{2v})	$^2A_1$	TlH: 1.864	0.0	TlH_2: 1483.4 (b_2, 605), 1353.9 (a_1, 173), 591.3 (a_1, 110)
		HTlH:		TlD_2: 1053.3 (305), 958.6 (87), 419.9 (55)
TlH_2^- (C_{2v})	$^1A_1$	TlH: 2.006	−31.1	TlH_2^-: 1011.8 (a_1, 1738), 1008.3 (b_2, 1839), 594.1 (a_1, 58)
		HTlH: 91.4		TlD_2^-: 717.6 (870), 715.0 (920), 421.2 (27)
$Tl^+(H_2)$ (C_{2v})	$^1A_1$	TlH: 3.004	103	$Tl^+(H_2)$: 4264.8 (a_1, 83), 232.7 (a_1, 20), 225.4 (b_2, 18)
		HH: 0.751		$Tl^+(D_2)$: 3016.8 (41), 165.4 (11), 159.5 (9)
TlH_2^+ ($D_{\infty h}$)	$^1\Sigma_g$	TlH: 1.674	151	TlH_2^+: 1994.7 (e_u, 9), 1883.8 (e_g, 0), 708.5 (π_u, 18 × 2)
		HTlH: 180.0		
TlH_3 (D_{3h})	$^1A_1'$	TlH: 1.744		TlH_3: 1685.1 (a_1', 0), 1668.4 (e′, 423 × 2), 647.1 (a_2'', 143), 583.6 (e′, 181)
		HTlH: 120.0		
TlH_4^- (T_d)	$^1A_1$	TlH: 1.818		TlH_4^-: 1479.6 (a_1, 0), 1382.4 (t_2, 927 × 3), 617.8 (e, 0 × 2), 578.8 (t_2, 504 × 3)
Tl_2H_2 (D_{2h})	^1A_g	TlH: 2.162	0.0	Tl_2H_2: 957.1 (a_g, 0), 922.3 (b_{1u}, 2003), 739.3 (b_{3g}, 0), 715.4 (b_{2u}, 424), 291.3 (b_{3u}, 11), 94.4 (a_g, 0)
		TlHTl: 109.5		Tl_2D_2: 677.2 (0), 654.0 (1007), 523.6 (213), 206.5 (5), 94.4 (0)
Tl_2H_2 (C_s)	$^1A'$	TlH: 1.853	12.1	Tl_2H_2: 1358.3 (a′, 1103), 952.7 (a′, 409), 638.3 (a′, 531), 336.9 (a′, 0), 205.6 (a″, 5), 66.6 (a′, 2)
		TlH′: 2.284		
		TlTl′: 3.179		
		HTlH′: 101.0		
Tl_2H_2 (C_{2h})	^1A_g	TlH: 1.870	18.3	Tl_2H_2: 1333.4 (b_u, 1861), 1323.3 (a_g, 0), 363.0 (a_g, 0), 146.1 (a_u, 45), 89.7 (b_u, 18), 56.1 (a_g, 0)
		TlTl: 3.199		
		HTlH: 121.8		
Tl_2H_2 (C_{2v})	$^1A_1$	TlH: 1.810	18.7	Tl_2H_2: 1459.1 (b_2, 650), 1448.7 (a_1, 939), 612.2 (a_1, 396), 302.3 (b_1, 66), 150.7 (b_2, 30), 87.8 (a_1, 3)
		TlTl′: 3.122		
		HTlH: 107.2		
Tl_2H_6 (D_{2h})	^1A_g	TlH: 2.026		Tl_2H_6: 1787.6 (b_{2u}, 598), 1777.1 (b_{1g}, 0), 1765.4 (a_g, 0), 1763.1 (b_{3u}, 162), 1143.7 (a_g, 0),
		TlH′: 1.711		1040.8 (b_{3u}, 1191), 985.3 (b_{2g}, 0), 909.8 (b_{1u}, 380), 635.7 (b_{2u}, 151), 617.9 (b_{3g}, 0),
		TlHTl: 100.1		586.1 (a_g, 0), 585.6 (b_{1u}, 82), 482.7 (b_{3u}, 809), 391.2 (b_{1g}, 0), 355.6 (a_u, 0), 210.0 (b_{2g}, 0),
		H′TlH′: 138.3		186.2 (b_{2u},0), 105.2 (a_g,0)

TABLE 3: Group 13 Metal Hydride Stretching Frequencies Observed in Solid Hydrogen[a−c]

	$M^+(H_2)_n$	$(H_2)MH_3$	M_2H_6	MH_3	M_2H_5	M_2H_4	MH_2	MMH_2	MH_4^-	MH	MH_2^-	M_2H_2	$(MH_3)_n$
Al	4108.7	4061.6	1932	1884	1918	1838	1822		1638	1599	(1430)	1156	1720
			1915		1845	1826	1788						
Ga	4108.9	4087.3	1995	1929	1967	1875	1815	1783	1774	1517	1356	1035	1900
			1976			1863	1746						1500
In	4113.1	4098.5	1820	1761		1707	1629	1530	1608	1393	(1225)	980	1460
			1803			1704	1563						
Tl	4113.6			1748			1520	1424		1311		909	
							1390						

[a] References 14−18. [b] $M^+(H_2)_n$ and $(H_2)MH_3$ are sharp bands for H−H ligand stretching frequencies. The AlH_2^- value is calculated from the AlD_2^- value in D_2 times the AlH_2/AlD_2 frequency ratio. $(MH_3)_n$ are solid film spectra. [c] The values for $B^+(H_2)_n$, 4089.3 cm^{-1}, and $B^+(D_2)_n$, 2940.4 cm^{-1}, are unpublished results from this laboratory.

structure is more stable than the linear $(HTlH)^+$ structure, but here we have a more highly coordinated Tl^+ species that is displaced 39.2 cm^{-1} below the 4152.8 cm^{-1} frequency for the solid n-H_2 lattice.[46] Finally, charge balance is achieved in these experiments by trapping H^- (D^-) in solid H_2 (D_2), as evidenced by strong 3972 (2870) cm^{-1} absorptions.[47]

Emission Spectra. Two properties of the 193 nm induced Tl emission spectra in solid H_2 and D_2 are interesting. In H_2, the two $^2S_{1/2} \rightarrow {}^2P_{1/2,3/2}$ components are blue-shifted 210 and 320 ± 20 cm^{-1}, and in solid D_2, these bands are blue-shifted 660 and 780 ± 20 cm^{-1}. Not only has D_2 blue-shifted the emissions ∼450 cm^{-1} more than H_2, but also the spin−orbit splitting (7793 cm^{-1} in the gas phase) has decreased by 120 ± 10 cm^{-1} in solid D_2 and by 110 ± 10 cm^{-1} in solid H_2. The smaller lattice parameter (3.600 Å) for solid n-D_2 suggests a more repulsive cage interaction than that for solid n-H_2 (3.769 Å).[48,49] Spin−orbit splitting is often diminished in the matrix,[50] and these small decreases (1.4−1.9%) are reasonable. Finally, the emission yield for Tl was much higher than that found for In and Ga in solid hydrogen, which attests the lower reactivity of Tl with H_2.

Reaction Mechanisms. The reactions of Tl and H_2 observed here are common to those for the other group 13 metals. The initial reaction (eq 1) is endothermic ($\Delta E = 58$ kcal/mol)[1] and must be driven by exciting the metal atom. The insertion reaction (eq 2) also requires activation energy. Note that $\lambda > 240$ nm irradiation (Figure 1b) markedly increases the yield of both TlH and TlH_2 and produces TlH_3 from reactions 3 and 4.

$$Tl + H_2 \rightarrow TlH + H \quad (1)$$

$$Tl + H_2 \rightarrow TlH_2 \quad (2)$$

$$TlH + H_2 \rightarrow TlH_3 \quad (3)$$

$$TlH_2 + H \rightarrow TlH_3 \quad (4)$$

Unreacted Tl clusters form Tl_2, and this reaction is favored in the soft neon matrix. Then irradiation leads directly to Tl_2H_2 formation (reaction 5). Such is the mechanism proposed for In_2H_2, but the reactions with Al_2 and Ga_2 are spontaneous. Note the experiments with HD in neon gave major Tl_2HD and those with $H_2 + D_2$ in neon favored Tl_2H_2 and Tl_2D_2 (Figure 5), which confirms the reduction in reaction 5. Very similar results are observed in solid argon (Figure 6). In the more rigid argon matrix at 3.5 K, unreacted Tl is isolated and H atoms from dissociation by laser plume radiation react upon annealing to form TlH, which also can dimerize (reactions 6 and 7). With higher laser energy, the yields of TlH and TlD from HD are large and the Tl_2H_2, Tl_2HD, and Tl_2D_2 yields from reaction 7 are statistical (Figure 6).

$$Tl_2 + H_2 \xrightarrow{UV} Tl_2H_2 \quad (5)$$

$$Tl + H \rightarrow TlH \quad (6)$$

$$2TlH \rightarrow Tl_2H_2 \quad (7)$$

Annealing in solid hydrogen fosters the further reaction of Tl with TlH_2, as reactions 1−3 require activation energy.

$$Tl + TlH_2 \rightarrow TlTlH_2 \quad (8)$$

The laser-ablation process produces metal cations as well as neutral atoms,[51] as seen from the emission spectrum (Figure 7), and the Tl^+ cation complex is formed upon trapping of Tl^+ in solid H_2.

$$Tl^+ + nH_2 \rightarrow Tl^+(H_2)_n \quad (9)$$

Conclusions

Laser-ablated Tl atoms react with H_2 much the same as In, Ga, and Al, but major differences do exist. Thallium is less reactive: The lower product band and higher 193 nm atomic emission yield attest this fact. The dominant thallium product is Tl(I)H, whereas the major aluminum product is Al(III)H_3. This substantiates the observation of Al_2H_6 and solid $(AlH_3)_n$ and the absence of Tl_2H_6 and solid $(TlH_3)_n$ in the product spectrum. Although the yield of TlH_3 is small, its identification with TlH_2D, $TlHD_2$, and TlD_3 isotopic modifications is definitive. Table 3 summarizes the group 13 metal hydride stretching frequencies: The TlH_3 fundamental is only 13 cm^{-1} below the InH_3 value, whereas the TlH_2 and TlH modes are 173−82 cm^{-1} below their indium counterparts.

The reaction of metal dimer M_2 with H_2 gives the rhombic M_2H_2 dimer, although the reactions are spontaneous for Al_2 and Ga_2 but they require photochemical activation for In_2 and Tl_2. A significant yield of the $TlTlH_2$ isomer is also observed. Sharp $^2S_{1/2} \rightarrow {}^2P_{1/2,3/2}$ emission from unreacted atomic Tl induced by 193 nm radiation is blue-shifted 660 cm^{-1} in solid D_2 and 210 cm^{-1} in solid H_2.

Although the DFT calculated electron affinity for TlH_2 is 32 kcal/mol, we have no definitive evidence for the TlH_2^- anion in the spectrum. This may arise from detachment by irradiation in the experiment. On the other hand, AlH_4^- is the dominant anion observed with Al.

The group 13 metal cations all form weak complexes with H_2 in the solid lattice with a H−H stretching mode 39−44 cm^{-1} below the solid H_2 fundamental at 4153 cm^{-1}.

Density functional theory using the relativistic SDD pseudopotential is adequate to calculate frequencies for thallium hydrides, but these calculations fit better for $TlH > TlH_2 > TlH_3$. However, relativistic MP2 calculations produce more accurate frequencies for TlH_3. It must be noted that the LANL2DZ pseudopotential and basis is vastly inferior for thallium hydrides.

Acknowledgment. We gratefully acknowledge support for this work from NSF Grant CHE 00-78836.

References and Notes

(1) Huber, K. P.; Herzberg, G. *Constants of Diatomic Molecules*; Van Nostrand: Princeton, NJ, 1979.

(2) Deutsch, J. L.; Neil, W. S.; Ramsay, D. A. *J. Mol. Spectrosc.* **1987**, *125*, 115.

(3) Zhu, Y. F.; Shehadeh, R.; Grant, E. R. *J. Chem. Phys.* **1992**, *97*, 883.

(4) Urban, R. D.; Magg, U.; Jones, H. *Chem. Phys. Lett.* **1989**, *154*, 135.

(5) Urban, R. D.; Birk, H.; Polomsky, P.; Jones, H. *J. Chem. Phys.* **1991**, *94*, 2523.

(6) Campbell, J. M.; Dulick, M.; Klapstein, D.; White, J. B.; Bernath, P. F. *J. Chem. Phys.* **1993**, *99*, 8379.

(7) Bahnmaier, A. H.; Urban, R. D.; Jones, H. *Chem. Phys. Lett.* **1989**, *155*, 269.

(8) White, J. B.; Dulick, M.; Bernath, P. F. *J. Mol. Spectrosc.* **1995**, *169*, 410.

(9) Ito, F.; Nakanaga, T.; Tako, H. *J. Mol. Spectrosc.* **1995**, *169*, 421.

(10) Chertihin, G. V.; Andrews, L. *J. Phys. Chem.* **1993**, *97*, 10295.

(11) Kurth, F. A.; Eberlein, R. A.; Schnöckel, H.; Downs, A. J.; Pulham, C. R. *J. Chem. Soc., Chem. Commun.* **1993**, 1302.

(12) Pullumbi, P.; Mijoule, C.; Manceron, L.; Bouteiller, Y. *Chem. Phys.* **1994**, *185*, 13.

(13) Pullumbi, P.; Bouteiller, Y.; Manceron, L.; Mijoule, C. *Chem. Phys.* **1994**, *185*, 25.

(14) Andrews, L.; Wang, X. *Science* **2003**, *299*, 2049.

(15) Wang, X.; Andrews, L.; Tam, S.; DeRose, M. E.; Fajardo, M. E. *J. Am. Chem. Soc.* **2003**, *125*, 9218.

(16) Andrews, L.; Wang, X. *J. Phys. Chem. A*, in press ($Al + H_2$).

(17) Wang, X.; Andrews, L. *J. Phys. Chem. A* **2003**, *107*, 11371 ($Ga + H_2$).

(18) Wang, X.; Andrews, L. *J. Phys. Chem. A*, in press ($In + H_2$).

(19) Knight, L. B., Jr.; Woodward, J. R.; Kirk, T. J.; Arrington, C. A. *J. Chem. Phys.* **1993**, *97*, 1304.

(20) (a) Larsson, T.; Neuhaus, H. *Ark. Fys.* **1963**, *23*, 461. (b) Urban, R.-D.; Bahnmaier, A. H.; Magg, U.; Jones, H. *Chem. Phys. Lett.* **1989**, *158*, 443.

(21) Christiansen, P. A.; Balasubramanian, K.; Pitzer, K. S. *J. Chem. Phys.* **1982**, *76*, 5087.

(22) (a) Balasubramanian, K.; Tao, J. X. *J. Chem. Phys.* **1991**, *94*, 3000. (b) Rakowitz, F.; Mirian, C. M. *Chem. Phys.* **1997**, *225*, 223.

(23) (a) Faegri, K.; Visscher, L. *Theor. Chem. Acc.* **2001**, *105*, 265. (b) Titov, A. V.; Mosyagin, N. S.; Alkseyev, A. B. *Int. J. Quantum Chem.* **2001**, *81*, 409.

(24) (a) Han, Y.-K.; Bae, C.; Lee, Y. S. *J. Chem. Phys.* **1999**, *110*, 9353. (b) Choi, Y. J.; Han, Y. K.; Lee, Y. S. *J. Chem. Phys.* **2001**, *115*, 3448.

(25) Schwerdtfeger, P.; Heath, G. A.; Dolg, M.; Bennett, M. A. *J. Am. Chem. Soc.* **1992**, *114*, 7518.

(26) Hunt, P.; Schwerdtfeger, P. *Inorg. Chem.* **1996**, *35*, 2085.

(27) Andrews, L.; Citra, A. *Chem. Rev.* **2002**, *102*, 885.

(28) Wang, X.; Andrews, L. *J. Phys. Chem. A* **2003**, *107*, 570.

(29) Wang, X.; Andrews, L. *J. Am. Chem. Soc.* **2003**, *125*, 6581 ($Pb + H_2$).

(30) Wang, X.; Souter, P. F.; Andrews, L. *J. Phys. Chem. A* **2003**, *107*, 4244 ($Bi + H_2$).

(31) Frisch, M. J.; Trucks, G. W.; Schlegel, H. B.; Scuseria, G. E.; Robb, M. A.; Cheeseman, J. R.; Zakrzewski, V. G.; Montgomery, J. A., Jr.; Stratmann, R. E.; Burant, J. C.; Dapprich, S.; Millam, J. M.; Daniels, A. D.; Kudin, K. N.; Strain, M. C.; Farkas, O.; Tomasi, J.; Barone, V.; Cossi, M.; Cammi, R.; Mennucci, B.; Pomelli, C.; Adamo, C.; Clifford, S.; Ochterski, J.; Petersson, G. A.; Ayala, P. Y.; Cui, Q.; Morokuma, K.; Malick, D. K.; Rabuck, A. D.; Raghavachari, K.; Foresman, J. B.; Cioslowski, J.; Ortiz, J. V.; Baboul, A. G.; Stefanov, B. B.; Liu, G.; Liashenko, A.; Piskorz, P.; Komaromi, I.; Gomperts, R.; Martin, R. L.; Fox, D. J.; Keith, T.; Al-Laham, M. A.; Peng, C. Y.; Nanayakkara, A.; Gonzalez, C.; Challacombe, M.; Gill, P. M. W.; Johnson, B.; Chen, W.; Wong, M. W.; Andres, J. L.; Gonzalez, C.; Head-Gordon, M.; Replogle, E. S.; Pople, J. A. *Gaussian 98*, revision A.7; Gaussian, Inc.: Pittsburgh, PA, 1998.

(32) (a) Becke, A. D. *J. Chem. Phys.* **1993**, *98*, 5648. (b) Stevens, P. J.; Devlin, F. J.; Chablowski, C. F.; Frisch, M. J. *J. Phys. Chem.* **1994**, *98*, 11623.

(33) (a) Krishnan, R.; Binkley, J. S.; Seeger, R.; Pople, J. A. *J. Chem. Phys.* **1980**, *72*, 650. (b) Frisch, M. J.; Pople, J. A.; Binkley, J. S. *J. Chem. Phys.* **1984**, *80*, 3265.

(34) (a) Becke, A. D. *Phys. Rev. A* **1988**, *38*, 3098. (b) Perdew, J. P. *Phys. Rev. B* **1983**, *33*, 8822. (c) Perdew, J. P.; Wang, Y. *Phys. Rev. B* **1992**, *45*, 13244.

(35) Milligan, D. E.; Jacox, M. E. *J. Mol. Spectrosc.* **1973**, *46*, 460.

(36) Wight, C. A.; Ault, B. S.; Andrews, L. *J. Chem. Phys.* **1976**, *65*, 1244.

(37) Moore, C. E. *Atomic Energy Levels*; Circular 467; National Bureau of Standards: Washington, DC, 1952.

(38) Line Spectra of the Elements. *CRC Handbook*, 66th ed.; Boca Raton, FL, 1985.

(39) Wiberg, E.; Dittmann, O.; Nöth, H.; Schmidt, M. *Z. Naturforsch. B* **1957**, *12*, 61.

(40) Wiberg, E.; Amberger, E. *Hydrides of the Elements of Main Groups I–IV*; Elsevier: Amsterdam, The Netherlands, 1971.

(41) Himmel, H.-J.; Manceron, L.; Downs, A. J.; Pullumbi, P. *J. Am. Chem. Soc.* **2002**, *124*, 4448.

(42) Igel-Mann, G.; Flad, H. J.; Feller, C.; Preuss, H. *THEOCHEM* **1990**, *209*, 313.

(43) Schwerdtfeger, P. *Inorg. Chem.* **1991**, *30*, 1660.

(44) Treboux, G.; Barthelat, J. C. *J. Am. Chem. Soc.* **1993**, *115*, 4870.

(45) Chen, Y.; Hartmann, M.; Diedenhofen, M.; Frenking, G. *Angew. Chem., Int. Ed.* **2001**, *40*, 2052.

(46) Gush, H. P.; Hare, W. F. J.; Allin, E. F.; Welsh, H. L. *Can. J. Phys.* **1960**, *38*, 176.

(47) Wang, X.; Andrews, L. *J. Phys. Chem. A* **2004**, *108*, 1103 (H^-).

(48) Krupskii, I. N.; Prokhvatilov, A. I.; Shcherbakov, G. N. *Low Temp. Phys. (Kiev)* **1983**, *9*, 446.

(49) Shcherbakov, G. N. *Sov. J. Low Temp. Phys.* **1991**, *17*, 73.

(50) (a) Vala, M.; Zerlinque, K.; ShakhsEmampour, J.; Rivoal, J.-C.; Pyzalski, R. *J. Chem. Phys.* **1984**, *80*, 2401. (b) Rose, J.; Smith, D.; Williamson, B. E.; Schatz, P. N.; O'Brien, M. C. M. *J. Phys. Chem.* **1986**, *90*, 2608. (c) Pellow, R.; Vala, M. J. *J. Chem. Phys.* **1989**, *90*, 5612.

(51) Kang, H.; Beauchamp, J. L. *J. Phys. Chem.* **1985**, *89*, 3364.